Advances in Research
8(3): 1-17, 2016; Article no.AIR.26399
ISSN: 2348-0394, NLM ID: 101666096

SCIENCEDOMAIN *international*
www.sciencedomain.org

Steady MHD Fluid Flow in a Bifurcating Rectangular Porous Channel

W. I. A. Okuyade[1*] and T. M. Abbey[2]

[1]Department of Mathematics and Statistics, University of Port Harcourt, Port Harcourt, Nigeria.
[2]Applied Mathematics and Theoretical Physics Group, Department of Physics, University of Port Harcourt, Port Harcourt, Nigeria.

Authors' contributions

This work was carried out in collaboration between both authors. Author TMA designed the study, wrote the protocol and supervised the work. Author WIAO managed the literature searches, solved the problem and did the programming for the results under the guidance of author TMA. Author TMA managed the analyses of the results. Author WIAO wrote the first draft. Author TMA edited the manuscript. Both authors read and approved the final manuscript.

Article Information

DOI: 10.9734/AIR/2016/26399
Editor(s):
(1) José Alberto Duarte Moller, Center for Advanced Materials Research, Complejo Industrial Chihuahua, Mexico.
(2) Francisco Marquez-Linares, Full Professor of Chemistry, Nanomaterials Research Group, School of Science and Technology, University of Turabo, USA.
Reviewers:
(1) L. Animasaun Isaac, Federal University of Technology, Akure, Ondo State, Nigeria.
(2) C. Sulochana, Gulbarga University, India.
(3) Mohammad Ali, CUET, Bangladesh.
(4) Bhim Sen Kala, H. N. B. Garhwal University (Central University), Garhwal, Srinagar, India.
Complete Peer review History: http://www.sciencedomain.org/review-history/17387

Original Research Article

Received 15th April 2016
Accepted 9th June 2016
Published 30th December 2016

ABSTRACT

Steady MHD fluid flow in a bifurcating rectangular porous channel is presented. The governing nonlinear equations are solved analytically by the methods of similarity transformation and regular perturbation series expansions. Expressions for the temperature, concentration and velocity are obtained and analyzed graphically. The results show that increase in bifurcation angle and Grashof numbers increase the transport velocity, whereas the increase in the magnetic field parameter decreases it. Furthermore, it is seen that an increase in bifurcation angle increases the temperature of the flow.

**Corresponding author: E-mail: wilsonia6011@gmail.com;*

Keywords: Bifurcation; MHD; porous channel; perturbation method; similarity transformation; steady flow.

1. INTRODUCTION

The flow of viscous incompressible fluid in both bifurcating and non-bifurcating porous channels has gained considerable attention in the past decades because of its practical applications in industries and engineering. Based on this, a good number of theoretical and experimental investigations relevant to this domain of research have been carried out. The concept of bifurcation (in sense that a flow system divides into two or more daughter channels) is seen in both natural and artificial settings. Therefore, it has applications in both science and engineering. It is relevant in biomechanics, astrophysics, hydrology, civil, electrical, petroleum engineering, and the likes. [1] studied the flow in a bifurcating cylindrical pipe using the visualization method, and observed that separation or reversal flow occurs at the outside wall of the junction. [2] studied the flow using the visualization approach, and observed that if the flow rates in the daughter tubes are unequal, separate reading occurs at the outer wall of the tube with a smaller flow rate. Also, [3] introduced the use of theoretical approach or mathematical tools in the study of branching flows. More so, [4] using the dye injection approach found that the critical Reynolds number at which turbulence developed in the glass model bifurcation depended on the angle of bifurcation. [5] used the hot-wire anemometer method to extend the work of [2]. They measured the velocity profile only in the steady flow and in the plane of bifurcation, and observed that the best measurements were those made with a hot-wire anemometer in the right angled model, and that flow separation was clearly present at one diameter from the junction. Furthermore, [6] examined the stabilities and bifurcation of a two-dimensional channel flow using analytic, numerical and experimental methods, and observed that flow separation occurs near the wall, and that both separation and bifurcation do not occur together. [7] investigated the three-dimensional symmetric one- to-two bifurcation using the analytic approach, and noticed that a flow separation or reversal occurs at the junction. Also, [8] studied the effect of bifurcation angles on the steady flow structure in a straight terminal aneurysm model with asymmetric outflow through the branches using the Laser-Doppler velocity and fluctuating intensity distribution. They observed that the size of the recirculation zones in the afferent vessel, the flow activity inside the aneurysm, and the shear stress acting on the aneurismal wall increase as the bifurcation angle increases. [9] conducted a numerical study on the effect of expansion ratio of the downstream: upstream on the flow, and was able to demonstrate the critical Reynolds number for asymmetric flow to occur. [10] investigated fluid flow through networks with two different types of geometries. This first is a tree of up to five generations of branches with no loops. The second is a tree of up to nine generations of identical channels that form a subset of a hexagonal lattice with loops. For the first type of geometry they showed that in spite of the symmetry of the structure, the flow distribution in the last generation becomes highly heterogeneous at high Reynolds number. For the tree with loops, they demonstrated that the profile of outflow fluxes at low values of Reynolds number can be adequately represented by the distribution of electric current exiting in an analog resistor network model. They observed that the flow at the outflow section depends on the velocity at the inlet, and tends to become more homogeneous as the Reynolds number is increased. [11] studied numerically and experimentally the steady aspiratory and expiratory flow in a three-dimensional airway system of single symmetric bifurcation. They showed that the flow results obtained from computational simulations are in good agreement with the experimental results, especially during expiration. [12] investigated numerically the steady respiratory flow through two-dimensional air way model with three generations of branches. They were able to confirm previous experimental observations, revealing a significant imbalance in the flow distribution between medial and lateral branching. [13] examined theoretically the behaviour of an incompressible side-branching flow at high Reynolds number and compared their results with those of direct numerical simulation at moderate Reynolds number. They observed that near the branch, the flow adjusts to the imposed downstream pressure in the daughter through a jump in the flow properties across the daughter entrance and that for large pressure drops in the daughter tube, the fluid is sucked in at high velocities from the mother and thereby provides a favourable upstream feedback. [14] investigated the equilibrium configuration and stability of a channel bifurcation in braided rivers, and showed that an increase in bifurcation angle increases

the transport velocity. More so, [15] showed that changes in bifurcation angle alter the flow condition and changes the magnitude of the wall shear stress. [16] investigated a three-dimensional one-to-two symmetrical flow in which the mother is straight and of circular cross-section, containing a fully developed incident motion, while the diverging daughters are straight and of semi-circular cross-section. Using the method of direct numerical simulation and slender modeling for a variety of Reynolds number and divergent angles, and observed that a flow separation or reversal occurs at the corners of the junction; the inlet pressure increases as the bifurcation angle increases. [17] studied blood flow in bifurcating arteries using the method of regular perturbation, and noticed that an increase in bifurcation angle and Reynolds number increase the transport velocity factor. Similarly, [18] examined the fluid-mechanical aspect of the flow in bifurcating arteries, and observed that an increase in bifurcation angle and Reynolds number produces a commensurate increase in the wall shear stress.

Furthermore, the flow through porous media is prevalent in nature and artificial settings. Therefore, it is of principal interest in science and engineering. It has relevance in petroleum engineering for the study of the movement of natural gas, oil and water through the oil reservoirs; in chemical engineering for filtration of and purification processes; in hydrology for studying the underground water resources. [19] examined free convective flow between a fluid and a porous layer in a rectangular enclosure; [20] investigated the flow in a rotating straight pipe and showed that the Nusselt number increases with increase in porosity. [21] studied the flow in a curved porous channel with rectangular cross-section filled with a fluid saturated porous medium, the flow being driven by a constant azimuthally pressure gradient, and using a generalized Fourier series method of solution found that the velocity profiles depend on the geometry of the channel and Darcy number. [22] presented an exact solution of the Navier-Stoke's equation for the steady flow of an incompressible viscous fluid along a channel with rigid porous walls, the flow being driven by uniform suction and injection at the wall. Using the Hiemenz similarity solution, the problem was reduced to a fourth order non-linear ordinary differential equation with a pair of boundary conditions at the wall. [23] investigated the slow flow of viscous incompressible liquid a channel of constant but arbitrary cross-sectional shape, driven by a non-uniform suction or injection through the porous channel walls using similarity transformation, and obtained results that provided a general framework for extending [22].

More so, the study of the flow of fluid through porous media has also been extended to include the effect of magnetic field. [24] examined analytically and numerically the unsteady magneto-hydrodynamic porous media flow through circular pipes and parallel plates, and observed that an increase in the porosity parameter accelerated the flow, and that the unsteady motion turned into a steady flow after a considerable lapse of time. [25] considered the flow of viscous incompressible fluid embedded with small spherical particles in a non-conducting channel with hexagonal cross-section in the presence of a transverse magnetic field using the method of integral transformation, and noticed that the velocity of the fluid and particles decrease with increase in the intensity of magnetic field. [26] investigated the effect of magnetic field on the flow in a rectangular enclosure using perturbation technique, and reported that the imposed magnetic field diminished the wall shear. [27] studied a two-dimensional flow of an incompressible viscous fluid flow through a non-porous channel with heat generation and chemical reaction by the methods of similarity transformation, homotopy analysis and numerical. They saw that an increase in the Reynolds number decreases the tangential velocity but increases the heat and mass transfer; the increases in the Eckert number and heat generation/absorption parameter increase temperature; the increase in the chemical reaction parameter decreases the concentration profiles, and the increase in the Grashof number increases the flow velocity. [28] examined the influence of magnetic field on the skin friction factor in a steady fully developed laminar flow through a pipe using the experimental and finite difference numerical scheme. They observed that the pressure drop varies in proportion to the square of the magnetic field and the sine angle; the pressure is proportional to the flow rate, and that the axial velocity asymptotically approaches its limit as the Hartmann number becomes large.

Similarly, magneto-hydrodynamic convective heat and mass transfer in porous and non-porous media is of considerable interest in technical field due to its applications in industries, geothermal, high temperature plasma, liquid metal and MHD power generating systems. [29]

examined the hydro magnetic natural convection flow through a horizontal permeable cylinder, and obtained a numerical solution of the non-similar boundary layer problem. [30] examined the fully developed free convection two-fluid magneto-hydrodynamic flow in an inclined channel using the perturbation techniques, and found that the flow can be controlled effectively by suitable adjustment of the values for the ratios of heights, electrical conductivities and viscosities of the two fluids. [31] studied the free convection flow through a vertical porous channel in the presence of an applied magnetic field using the finite difference numerical approach, and noticed that the velocity decreases with the increase in the magnetic and porosity parameters throughout the region. [32] investigated the effects of magnetic field and convective force on the flow in bifurcating porous fine capillaries, and found that magnetic field reduces the flow velocity, whereas the convective force increases it. [33] considered the fully developed mixed convection flow in a vertical channel filled with nano-fluids in the presence of a uniform transverse magnetic field using closed form solutions. They noticed that magnetic field enhances the nano-fluid velocity in the channel; the induced magnetic field vanishes in the central region of the channel; the critical Raleigh number at the onset of the instability of flow is strongly dependent on the volume fraction of nano-particles and the magnetic field. More so, [34] examined blood flow in bifurcating arteries analytically, and observed that an increase in heat exchange parameter and Grashof number increase the velocity, concentration and Nusselt number of the flow, while an increase in the heat exchange parameter increases the Sherwood number.

An examination of most of the previous studies on the flow in bifurcating channels shows that the problem was particularized to certain fields. They applied it to arterial blood flow, bronchial air flow, streams and rivers, biomechanics of green plants, and the likes. Therefore, the purpose of this study is to present a generalized model of the steady MHD flow of fluid in bifurcating rectangular porous channels. In view of this, this study examines the effects of bifurcation angle, environmental thermal differentials, and magnetic field on the flow field.

The paper is organized in the following format: section 2 is the methodology; section 3 holds the results and discussion, while section 4 gives the conclusions.

2. METHODOLOGY

The problem is formulated based on the following assumptions: that the channel is permeable; the fluid is incompressible, Newtonian, electrically conducting and chemically reacting (but of the homogeneous first order type i.e. the reaction is directly proportional to the concentration). We also assume that the bifurcating channels are symmetrical. Therefore, if (u', v', w') are the velocity vectors with respect to the orthogonal Cartesian coordinates (x', y', z') and are symmetrical about the z' axis such that the variations about z' is zero, the velocity and coordinate vectors become (u', v') and (x', y') respectively; then the mathematical models for the continuity, momentum, energy and diffusion equations, using the Boussinesq approximations are:

$$\frac{\partial u'}{\partial x'} + \frac{\partial v'}{\partial y'} = 0 \tag{1}$$

$$u'\frac{\partial u'}{\partial x'} + v'\frac{\partial u'}{\partial y'} = -\frac{1}{\rho'}\frac{\partial p'}{\partial x'} + \frac{\mu}{\rho'}\left(\frac{\partial^2 u'}{\partial x'^2} + \frac{\partial^2 u'}{\partial y'^2}\right) + g\beta_t\left(T' - T_\infty\right) + g\beta_c\left(C' - C_\infty\right) - \frac{\sigma_e B_o^2 u'}{\rho'^2 \mu_m} - \frac{\upsilon u'}{\kappa} \tag{2}$$

$$u'\frac{\partial v'}{\partial x'} + v'\frac{\partial v'}{\partial y'} = -\frac{1}{\rho'}\frac{\partial p'}{\partial y'} + \frac{\mu}{\rho'}\left(\frac{\partial^2 u'}{\partial x'^2} + \frac{\partial^2 u'}{\partial y'^2}\right) \tag{3}$$

$$u'\frac{\partial T'}{\partial x'} + v'\frac{\partial T'}{\partial y'} = -\frac{1}{\rho'}\frac{k_o}{C_p}\left(\frac{\partial^2 T'}{\partial x'^2} + \frac{\partial^2 T'}{\partial y'^2}\right) + \frac{1}{\rho'}\frac{Q}{C_p}\left(T' - T_\infty\right) \tag{4}$$

$$u\frac{\partial C'}{\partial x'}+v'\frac{\partial C'}{\partial y'} =-\frac{D}{\rho'}\left(\frac{\partial^2 C'}{\partial x'^2}+\frac{\partial^2 C'}{\partial y'^2}\right)+\frac{k_r^2}{\rho'}\left(C'-C_\infty\right) \quad (5)$$

where β_t and β_c ar the volumetric expansion coefficient for temperature and concentration respectively; T' fluid temperature; T_∞ temperature at equilibrium; C' concentration (quantity of material being transported); C_∞ concentration at equilibrium; **g** gravitational field vector; p' pressure; ρ' density of the fluid; μ viscosity of the fluid; μ_m magnetic permeability of the fluid; κ is the permeability of the porous medium; B_o^2 is the applied uniform magnetic field strength due the nature of the fluid; σ_e is the electrical conductivity of the fluid; k_o the thermal conductivity; C_p the specific heat capacity at constant pressure; Q is the heat absorption coefficient; D the diffusion coefficient; k_r^2 is the rate of chemical reaction of the fluid, which is homogeneous and of order one.

The model in Figure 1 shows that the channel is assumed to be symmetrical and divided into two regions: the upstream (or mother) region $x'< x_o$ and downstream (or daughter) region $x'> x_o$, where x_o is the bifurcation or the nodal point, which is assumed to be the origin such that the stream boundaries become $y'=\pm d$ for the upstream region and $y'=\alpha x'$ for the downstream region. Due to geometrical transition between the mother and daughter channels, the problem of wall curvature effect is bound to occur. To fix up this, a very simple transition wherein the width of the daughter channel is made equal to half that of the mother channel i.e. $\pm d$ is such that the variation of the bifurcation angle is straight-forwardly used (see [16]).

Furthermore, if the width of the channel ($2d$) is far less than its length (l_o) before the point of bifurcation such that the ratio of $\frac{2d}{l_o}=\Re<<1$, (where $\Re$ is the aspect ratio), the flow is laminar and Poiseuille (see[35]). d is assumed to be non-dimensionally equal to one (see [16]). Similarly, at the entry region of the mother channel, the flow velocity is given as $u'=U_o\left(1-y'^2\right)$, where U_o is the characteristic velocity, which is taken to be maximum at the centre and zero at the wall (see [16]). Based on the above, the boundary conditions become:

$$u'=1, v'=0,\ T'=1, C'=1 \text{ at } y'=0 \quad (6)$$

$$u'=0, v'=0, T'=T_w,\ C'=C_w \text{ at } y'=1 \quad (7)$$

for the upstream/mother channel

$$u'=0, v'=0, T'=0, C'=0 \text{ at } y'=0 \quad (8)$$

$$u'=0, v'=0,\ T'=\gamma_1 T_w,\ C'=\gamma_2 C_w,\ \gamma_1<1,\ \gamma_2<1 \text{ at } y'=\alpha x' \quad (9)$$

for the downstream/daughter channel

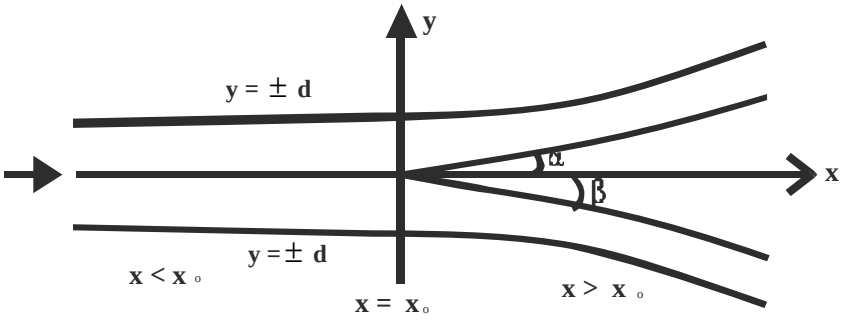

Figure 1. A bifurcating symmetrical rectangular channel (with α=β, α and β are the bifurcation angles)

Introducing the following non-dimensional variables:

$$x=\frac{x'}{\ell_c},\ y=\frac{y'}{\ell_c},\ u=\frac{u'}{U_o},\ v=\frac{v'}{U_o},\ p=\frac{p'}{p_\infty},\ \rho=\rho' U_o^2,\ \Theta=\frac{T'-T_\infty}{T_w-T_\infty},\Phi=\frac{C'-C_\infty}{C_w-C_\infty},$$

$$\upsilon=\frac{\mu}{\rho},\mathrm{Re}=\frac{\rho U_o \ell_c}{\mu},Gr=\frac{\rho g\beta_t(T_w-T_\infty)\ \ell_c^2}{\mu U_o}\quad Gc=\frac{\rho g\beta_c(C_w-C_\infty)}{\mu U_o},\chi^2=\frac{\ell_c^2}{\kappa},$$

$$\delta_1^2=\frac{k_r^2\ell_c^2}{D},\quad M^2=\frac{\sigma_e B_o^2\ \ell_c^2}{\rho\mu\mu_m},\quad N^2=\frac{Ql_c^2}{k_o},\ Sc=\frac{\mu}{\rho D}$$

where ℓ_c is the scale length; p_∞ is ambient/equilibrium pressure; C_w constant wall temperature at which the channel is maintained; T_w constant wall concentration at which the channel is maintained; Θ is the dimensionless temperature; Φ is the dimensionless concentration; υ is the kinematic viscosity; Re is the Reynolds number; Gr is the Grashof number due to temperature difference; Gc is the Grashof number due to concentration difference; χ^2 is the local Darcy number; M^2 is the Hartmann's number; Pr is the Prandtl number; Sc is the Schmidt number; and δ_1^2 is the rate of chemical reaction; N^2 is the heat exchange parameter; into equations (1) - (8),we have

$$\frac{\partial u}{\partial x}+\frac{\partial v}{\partial y}=0 \tag{10}$$

$$\mathrm{Re}\left(u\frac{\partial u}{\partial x}+v\frac{\partial u}{\partial y}\right)=-\frac{\partial p}{\partial x}+\left(\frac{\partial^2 u}{\partial x^2}+\frac{\partial^2 u}{\partial y^2}\right)+Gr\Theta+Gc\Phi-\chi^2 u-M^2 u \tag{11}$$

$$\mathrm{Re}\left(u\frac{\partial v}{\partial x}+v\frac{\partial v}{\partial y}\right)=-\frac{\partial p}{\partial y}+\left(\frac{\partial^2 v}{\partial x^2}+\frac{\partial^2 v}{\partial y^2}\right) \tag{12}$$

$$\mathrm{Re}\,\mathrm{Pr}\left(u\frac{\partial \Theta}{dx}+v\frac{\partial \Theta}{\partial y}\right)=\left(\frac{\partial^2 \Theta}{dx^2}+\frac{\partial^2 \Theta}{\partial y^2}\right)+N^2\Theta \tag{13}$$

$$\mathrm{Re}\,Sc\left(u\frac{\partial \Phi}{dx}+v\frac{\partial \Phi}{\partial y}\right)=\left(\frac{\partial^2 \Phi}{dx^2}+\frac{\partial^2 \Phi}{\partial y^2}\right)+\delta_1^2\Phi \tag{14}$$

with the boundary conditions

$$u=1,\ v=0,\Theta=1,\Phi=1\ \text{ at }\ y=0 \tag{15}$$

$$u=0,v=0,\Theta=\ \Theta_w,\ \Phi=\Phi_w\quad\text{at}\quad y=1 \tag{16}$$

for the upstream channel

$$u=0,v=0,\Theta=0,\Phi=0\quad\text{at}\quad y=0 \tag{17}$$

$$u=0,v=0,\ \Theta=\ \gamma_1\Theta_w,\ \ \Phi=\gamma_2\Phi,\ \gamma_1<1,\ \gamma_2<1\ \text{ at }\ y=\alpha x \tag{18}$$

for the downstream channel

Introducing the similarity solution:

$$\Psi = (U_o \upsilon x)^{1/2} f(\eta), \eta = \left(\frac{U_o}{\upsilon x}\right)^{1/2} y \quad (19)$$

with the velocity components represented as

$$u = \frac{\partial \Psi}{\partial y}, \quad v = -\frac{\partial \Psi}{\partial x} \quad (20)$$

where Ψ is the stream function and η is the similarity independent variable, into equations (10) - (18), we have the following equivalent equations

$$f''' = 0 \quad (21)$$

$$f''' + f'' - M_1^2 f' + \mathrm{Re}(f' f'' + f f'') = -Gr\,\Theta - Gc\,\Phi \quad (22)$$

$$\Theta'' + \Theta' + \mathrm{Re}\,\mathrm{Pr}(-f'\Theta' + f\,\Theta') + N^2\Theta = 0 \quad (23)$$

$$\Phi'' + \Phi' + Re\,Sc(-f'\Phi' + f\,\Phi') + \delta_1^2\Phi = 0 \quad (24)$$

where $M_1^2 = M^2 + \chi^2$

with the boundary indications:

$$f = 1, f' = 0, \Theta = 1, \Phi = 1 \quad \text{at } \eta = 0 \quad (25)$$

$$f' = 0, f = 0, \Theta = \Theta_w, \Phi = \Phi_w \quad \text{at } \eta = 1 \quad (26)$$

for the upstream channel

$$f = 0, f' = 0, \Theta = 0, \Phi = 0 \quad \text{at } \eta = 0 \quad (27)$$

$$f' = 0, f = 0, \Theta = \gamma_1\Theta_w, \Phi = \gamma_2\Phi_w, \quad \gamma_1 < 1, \gamma_2 < 1 \quad \text{at } \eta = ax \quad (28)$$

for the downstream channel

Equations (21) - (28) show that the similarity equations are coupled and highly non-linear. Therefore, to minimize the effect of non-linearity on the flow variables we introduce a perturbation series solution of the form

$$h(x, y) = h_o(x, y)) + \xi h_1(x, y) + \ldots \quad (29)$$

where $\xi = \frac{1}{\mathrm{Re}} << 1$ is the perturbing parameter. We choose this parameter because, almost at the point of bifurcation, due to a change in the geometrical configuration, the inertial force rises and the momentum increases. The increase in the momentum is associated with a drastic increase in the Reynolds number. In this regard, equations (21) - (28) become:

for the zeroth order:

$$f_o'' = 0 \quad (30)$$

$$f_o''' + f_o'' - M_1^2 f_o' = -Gr\Theta_o - Gc\Phi_o \quad (31)$$

$$\Theta_o'' + \Theta_o' + N^2\Theta_o = 0 \quad (32)$$

$$\Phi_o'' + \Phi_o' + \delta^2{}_1\Phi_o = 0 \quad (33)$$

with the boundary conditions

$$f_o = 1, f_o' = 0, f_o'' = 0, \Theta_o = 1, \Phi_o = 1 \text{ at } \eta = 0 \quad (34)$$

$$f_o = 0, f_o' = 0, f_o'' = 0, \Theta_o = 0, \Phi_o = 0 \text{ at } \eta = 1 \quad (35)$$

and for the first order:

$$f_1'' = 0 \quad (36)$$

$$f_1''' + f_1'' - M_1^2 f_1' = f_o' f_o'' - f_o f_o'' - Gr\Theta_1 - Gc\Phi_1 \quad (37)$$

$$\Theta_1'' + \Theta_1' + N^2\Theta_1 = \mathrm{Pr}(f_o'\Theta_o' - f_o\Theta_o') \quad (38)$$

$$\Phi_1'' + \Phi_1' + \delta_1^2\Phi_1 = Sc(f_o'\Phi_o' - f_o\Phi_o') \quad 39)$$

with the boundary conditions

$$f_1 = 0, f_1' = 0, \Theta_1 = 0, \Phi_1 = 0 \quad \text{at } \eta = 0 \quad (40)$$

$$f_1 = 0, f_1' = 0, \Theta_1 = \gamma_1\Theta_w, \Phi_1 = \gamma_2\Phi_w, \quad \gamma_1 < 1, \gamma_2 < 1 \quad \text{at } \eta = ax \quad (41)$$

The zeroth order equations describe the flow in the upstream channel, while the first order equations describe the flow in the downstream channels. More so, the presence of the zeroth order terms in the first order equations indicate the influence of the upstream on the downstream flow.

The solutions to equations (30) - (35) that is, for the upstream are:

$$\Theta_o(\eta) = \frac{\Theta_w e^{\frac{1}{2}(1-\eta)} \sinh \mu_1 \eta}{\sinh \mu_1} + \frac{e^{-\frac{1}{2}(1-\eta)} \sinh \mu_1 (1-\eta)}{\sinh \mu_1} \tag{42}$$

$$\Phi_o(\eta) = \frac{\Phi_w e^{\frac{1}{2}(1-\eta)} \sinh \mu_2 \eta}{\sinh \mu_2} + \frac{e^{-\frac{1}{2}(1-\eta)} \sinh \mu_2 (1-\eta)}{\sinh \mu_2} \tag{43}$$

$$f_o(\eta) = \frac{\left(f_{o(p)}(0) e^{-(\mu 3+\eta/2)} \sinh \mu_3 \eta \right)}{\sinh \mu_3} + \frac{\left(f_{o(p)}(1) e^{-1/2(1-\eta)} \sinh \mu_3 \eta \right)}{\sinh \mu_3}$$

$$- f_{o(p)}(0) e^{-(\mu_3+\eta/2)} + f_{o(p)}(\eta) \tag{44}$$

and those for equations (36) - (41), that is, for the downstream are

$$\Theta_1(\eta) = \frac{\gamma_1 \Theta_w e^{\frac{1}{2}(\alpha x-\eta)} \sinh \mu_1 \eta}{\sinh(\mu_1 \alpha x)} - \frac{\Theta_{1(p)}(\alpha x) e^{-\frac{1}{2}(\alpha x-\eta)} \sinh \mu_1 \eta}{\sinh(\mu_1 \alpha x)}$$

$$+ \frac{\Theta_{1(p)}(0) e^{-(\mu \alpha x+\eta/2)} \sinh \mu_1 \eta}{\sinh(\mu_1 \alpha x)} - \Theta_{1(p)}(0) e^{-(\alpha x-(\mu_1+1/2)\eta)} + \Theta_{1(p)}(\eta) \tag{45}$$

$$\Phi_1(\eta) = \frac{\gamma_2 \Phi_w e^{\frac{1}{2}(\alpha x-\eta)} \sinh \mu_2 \eta}{\sinh(\mu_2 \alpha x)} + \frac{\Phi_{1(p)}(\alpha x) e^{-\frac{1}{2}(\alpha x-\eta)} \sinh \mu_2 \eta}{\sinh(\mu_2 \alpha x)}$$

$$+ \frac{\Phi_{1(p)}(0) e^{-(\mu \alpha x+\eta/2)} \sinh \mu_2 \eta}{\sinh(\mu_2 \alpha x)} - \Phi_{1(p)}(0) e^{-(\alpha x-(\mu_2+1/2)\eta)} + \Phi_{1(p)}(\eta) \tag{46}$$

$$f_1(\eta) = \frac{f_{1(p)}(0) e^{-(\mu_3 \alpha x+\eta/2)} \sinh \mu_3 \eta}{\sinh \mu_3 \alpha x} + \frac{f_{1(p)}(\alpha x) e^{1/2(\alpha x-\eta)} \sinh \mu_3 \eta}{\sinh(\mu_3 \alpha x)}$$

$$- f_{1(p)}(0) e^{(\alpha x-(\mu_{3+1/2})\eta)} + f_{1(p)}(\eta) \tag{47}$$

3. RESULTS AND DISCUSSION

The computational results are obtained using Maple 12 computational software. We used the following realistic and constant values of $\gamma_1 = 0.6$, $\gamma_2 = 0.6$, $\Phi_w = 2.0$, $\Theta_w = 2.0$, $Pe_h = 0.07$, $Pe_m = 0.07$, Re= 400, Re=400, $\delta_1^2 = 0.2$, $N^2 = 0.2$, $\chi^2 = 0.2$ and varied values of α=5, 10, 15, 20; Gr/Gc=0.1, 0.3, 0.5, 1.0, 5.0 and M^2=0.1, 0.3, 0.5, 1.0, 10.0 to get the results below.

In this paper, we investigate the effects of bifurcation angle, Grashof number and magnetic field on the flow. To this end, Figures 2–10 illustrate the effects of these on the flow field. The results obtained, show that, for increase in the values of α and Gr/Gc, the temperature and transport velocity increase (see Figures 2–8), whereas the increase in M^2 decreases the velocity (see Figure 9) Furthermore, the increase in M^2 makes the velocity fluctuating (see Figure 10).

An increase in the angle of bifurcation narrows the width of the daughter channels, which in turn increases the inlet pressure, and consequently increases the velocity structure (see Figures 4 and 5). This is in agreement with [14,16, 17,18]. More so, as the velocity increases, the energy of the system which is a function of velocity increases, thus, accounting for what is seen in Figures 2 and 3.

Similarly, an increase in the external temperature produces a thermal differential between the flow system and its surrounding. The thermal differential in the presence of gravity and viscous factors produces convective currents, which serve as a lifting or buoyancy force to the fluid particles. Moreover, as the external temperature increases, heat is absorbed into the system. With the rise in the internal temperature, the viscous force drops such that the Reynolds number is increased. Consequent upon these, the flow velocity increases. And these account for what is seen in Figure 6-Figure 8. These results are in perfect agreement with [27,32,34].

On the other hand, the fluid being electrically conducting implies that it is magnetically susceptible. The action of the earth magnetic field on the fluid particles produces a mechanical force, the Lorentz force, which gives the flow a new orientation. In particular, the Lorentz force has a freezing impact on the velocity flow structure, thus accounting for what is seen in Figure 9. This result is in consonance with [25, 27,28,31,32]. Even so, the fluctuation, manifested in the form of back-and-forth movement of the fluid, as seen in Figure 10, possibly, seems partly due to the internal waves developed in the fluid in the flow process, or may be due to the interaction between the pressure force and the gravity force.

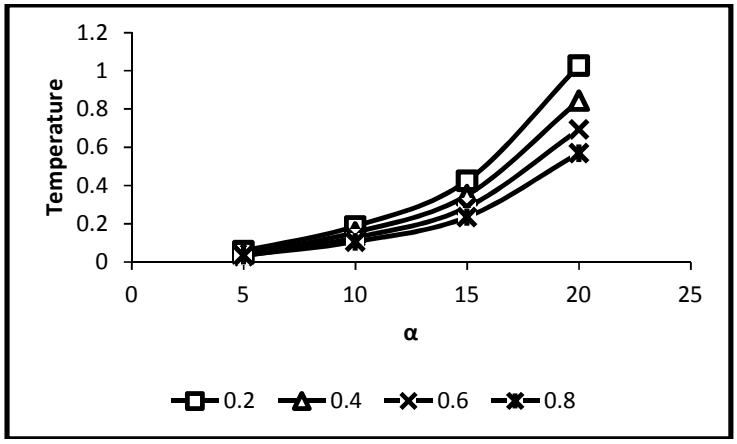

Figure 2. Temperature profiles for various bifurcation angles (α) in the daughter channel

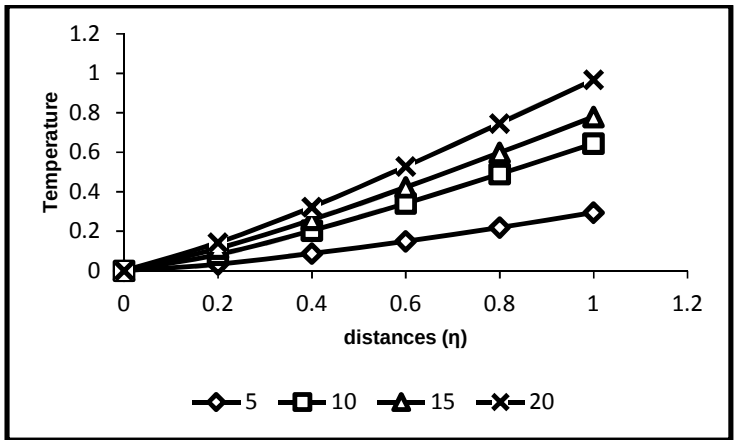

Figure 3. Temperature-bifurcation angle (α) profiles at various distances (η) in the daughter channel

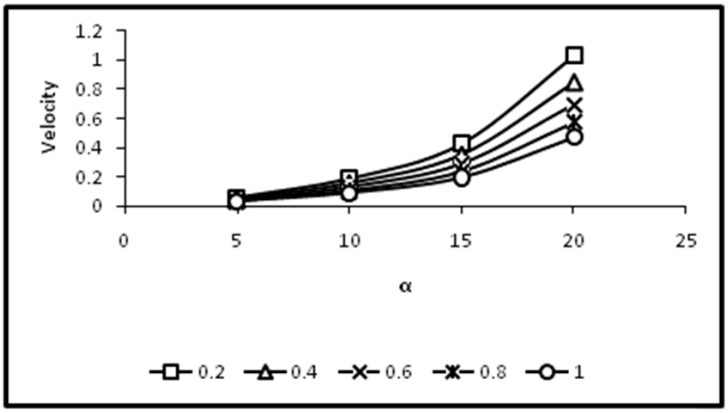

Figure 4. Velocity profiles for various bifurcation angles (α) in the daughter channel

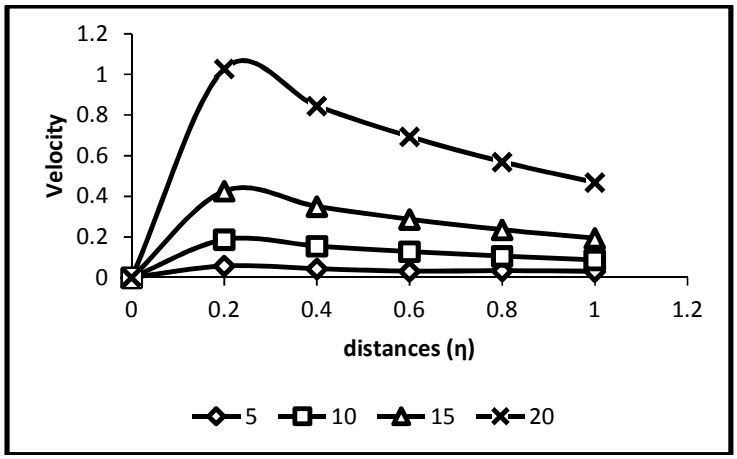

Figure 5. Velocity-bifurcation angle (α) profiles at various distances (η) in the daughter channel

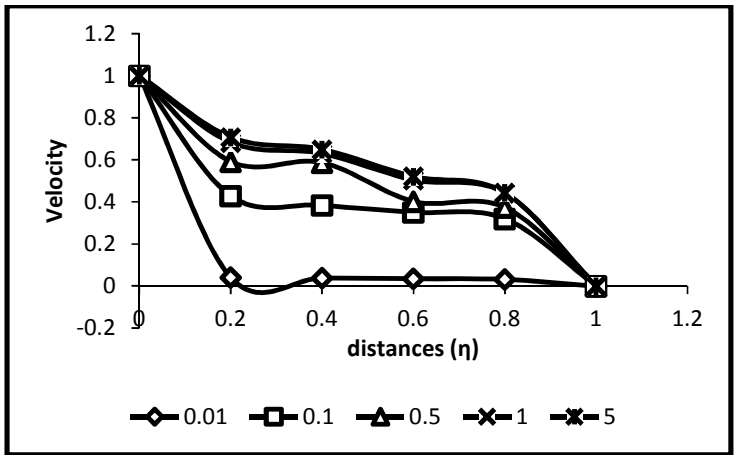

Figure 6. Velocity-Grashof number (Gr/Gc) profiles at various distances (η) in the mother channel

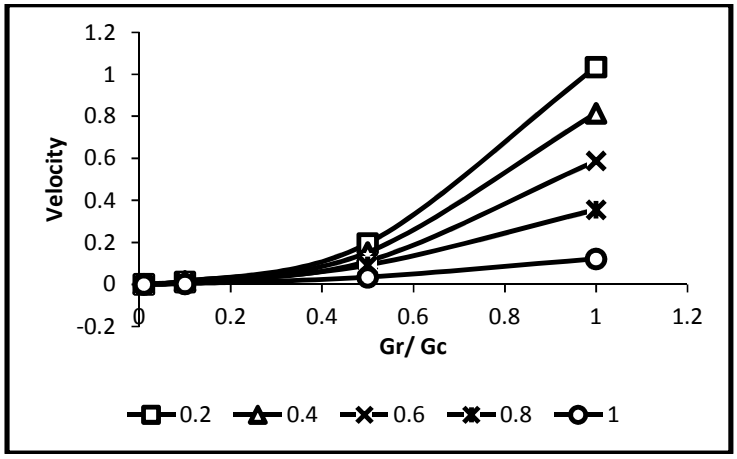

Figure 7. Velocity profiles for various Grashof numbers (Gr/Gc) in the daughter channel

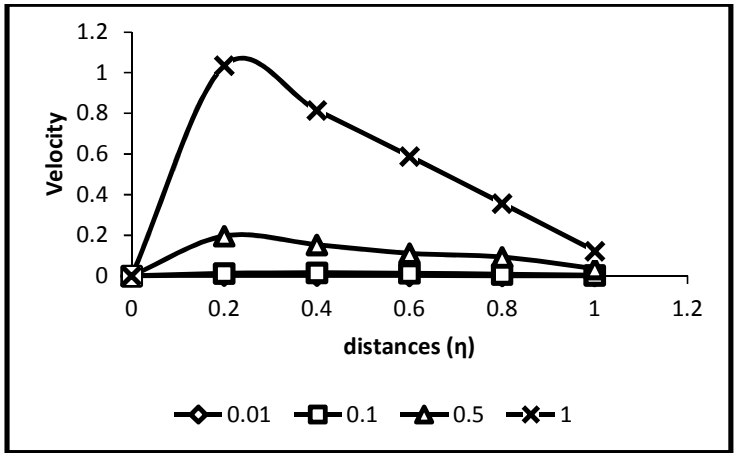

Figure 8. Velocity-Grashof numbers (Gr/Gc) profiles at various distances (η) in the daughter channel

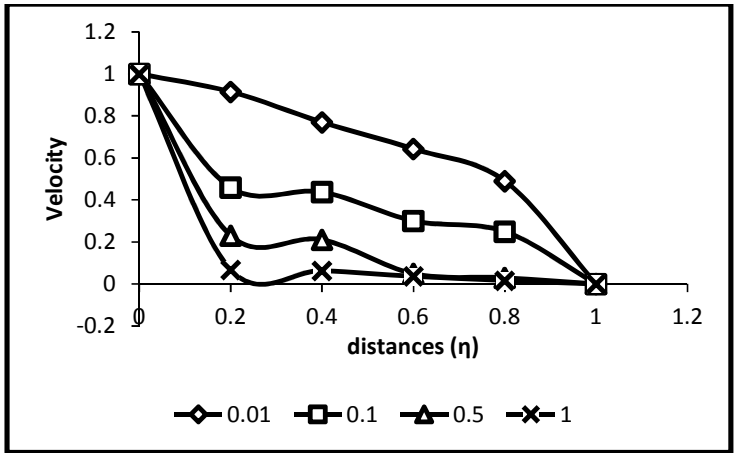

Figure 9. Velocity-magnetic field parameter (M^2) profiles at various distances (η) in the mother channel

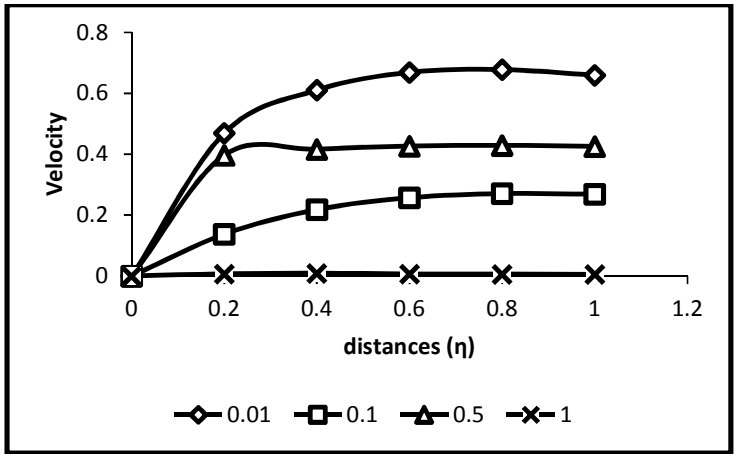

Figure 10. Velocity-magnetic field parameter (M^2) profiles at various distances (η) in the daughter channel

4. CONCLUSION

The flow of fluid in a bifurcating rectangular porous channel is investigated. The analyses of the flow model show that the temperature and velocity increase with bifurcation angle; the velocity increases with Grashof numbers, while the increase in magnetic field parameter reduces the transport velocity. Furthermore, the fluctuating motion of the fluid leads to loss of energy for the flow in the axial direction.

COMPETING INTERESTS

Authors have declared that no competing interests exist.

REFERENCES

1. Schroter R, Sudlow MJ. Flow patterns in models of the human bronchial airways. Respiratory Physiology. 1969;7:341-355.
2. Zeller H, Talukder N, Lorentz J. Model studies of pulsating flow in arterial branches and wave propagation in blood vessels: In fluid dynamics of circulatory flow. AGARD Conference Proceedings. 1970;65.
3. Pedley TJ, Schroter RC, Sudlow MF. The prediction of pressure drop and variation of resistance within the human bronchial airways. Resp. Physiology. 1970;9:387–405.
4. Roach MR, Scott S, Ferguson GG. Hemodynamic importance of geometry of bifurcations in circles of Willis glass model studies. Stroke. 1972;3:255-67.
5. Talukder N, Nerem RM. Flow characteristics in vascular graft model. Digest of first International Conference on Mechanics in Medicine and Biology, Aachen. 1978;vii:281–84.
6. Sobey J, Philip Drazin G. Bifurcating two-dimensional flow. J Fluid Mechanics. 1986;171:263-87.
7. Skalak Richard, Skalak Thomas, Nihat Ozkaya. Biofluid mechanics. Rev. Fluid Mechanics. 1989;21:167–204.
8. Liou TM, Change TW, Change WC. Effects of bifurcation angle on the steady flow structure in model saccular aneurysms. Experiments in Fluids. 1993;289–295.
9. Drikakis D. Bifurcation phenomena in an incompressible sudden expansion flow. Phys. Fluids. 1997;9:76–86.
10. Almeid MP, Andrade JS Jr., Budgrev SV, Cavalcante FSA, Stanley HE, Suki B. Fluid flow through ramified structure. Physical Review. 1999;60(50):5486–94.
11. Zhao Z, Leiber BB. Steady expiratory flow in a model symmetric bifurcation. J Biomech Eng. 1994;116:318–23.
12. Wilquem F, Degrez G. Numerical modeling of steady aspiratory airflow through a 3-generation model of the human central airways. ASME J Biomechanical Engineering. 1997;119:59–65.
13. Smith FT, Ovenden NC, Frank P, Doorly DJ. What happens to pressure when a fluid enters a side branch. J Fluid Mechanics. 2003;479:231–58.
14. Pittaluga MB, Repetto R, Tubino M. Channel bifurcation in braided rivers: Equilibrium configuration and stability.

Water Resources Research. 2003; 39(3):1046–57.
15. Soulis. J Biomech. 2004;39:742–49.
16. Tadjar M, Smith FT. Direct simulation and modeling of a 3-dimensional bifurcating tube flow. J Fluid Mechanics. 2004;519:1-32.
17. Okuyade WIA, Abbey TM. Analytic study of blood flow in bifurcating arteries, part 1-effects of bifurcating angle and magnetic field. International Organization of Scientific Research J Mathematics; 2015. I.D: G54040 - (in press).
18. Okuyade WIA, Abbey TM. Analytic study of blood flow in bifurcating arteries, part 3- on wall shear stress. International Organization of Scientific Research J Mathematics; 2015. I.D: G54041-(in press).
19. Beckermann C, Ramdhyani S, Viskanta R. Natural convection flow and heat transfer between a fluid layer and a porous layer inside a rectangular enclosure. J Heat Transfer. 1987;109:363–370.
20. Rao Ramana VV, Sobha VV. Heat transfer of a saturated porous flow in a rotating straight pipe. Proceeding of the Tenth National Heat and Mass Transfer Conference, Madurai Kamoraj University, Madurai. 1987;13.
21. Avramenko AA, Kuznetsov AV. Flow in a curved porous channel withrectangular cross-section. J Porous Media. 2008;241-48. DOI: 10.1615/JporMedia.v.11.i3.20
22. Berman AS. Laminar flow in channels with porous walls. J Applied Physics. 1963; 2(9):1232-36.
23. Jonson KH. Slow flow in channels with porous walls; 2012. arXiv.1208.5424Vi [Physics. Fluid-dyn].
24. Gulab R, Mishra S. Unsteady flow through magneto-hydrodynamic porous media. Indian J Pure, Applied Maths. 1977;8(6): 637–47.
25. Kaur JP, Singh GD, Sharma RG. Unsteady porous channel flow of a conducting fluid with suspended particles. Defence Science. 1988;38(1):13-20.
26. Abdel-Malek MB, Helal MM. Similarity solutions for magneto-force unsteady free convective laminar boundary–layer flow.J Comput. App. Maths. 2008;218:202–14.
27. Shateyi S, Motsa SS, Sibanda P. Homotopy analysis of heat and mass transfer boundary layer flow through a non-porous channel with chemical reaction and heat generation. The Canadian J Chemical Engineering. 2010;88:975-982.
28. Asadolah Malekzadeh, Amir Heydarinasab, Bahram Dabir. Magnetic field effect on fluid flow characteristic in a pipe for laminar flow. J Mechanical Sci. and Tech. 2011;25:333-39.
29. Chamkha AJ, Quadri MMA. J Heat Transfer. 2001;A40:387–401.
30. Malashetty MS, Umvati JS, Prathap Kumar J. Convective MHD flow heat transfer in an inclined channel. Heat and Mass Transfer. 2001;37:259-64.
31. Venkateswalu S, Suryanarayama Rao KV, Rambupal Reddy B. Finite difference analysis on convective heat transfer flow through porous medium in a vertical channel with magnetic field. Indian Journal of Applied Maths and Mechanics. 2011;7(7):74–94.
32. Okuyade WIA. MHD blood flow in bifurcating porous fine capillaries. African J Science Research. 2015;4(4):56-59.
33. Das S, Jana RN, Makinde OD. Mixed convection magnetohydrodynamic flow in a channel filled with nanofluids. Elsevier J Engineering Science and Technology. 2015;244-255. DOI:http://dx.doi.org/10.1016/j.jestch 2014.12009
34. Okuyade WIA, Abbey TM. Analytic study of blood flow in bifurcating arteries, part 2-effects of environmental temperature differentials. International Organization of Scientific Research J Mechanical Engineering; 2015. I.D: G54083 - (in press)
35. Bestman AR. Global models for the biomechanics of green plants, part 1. International J Energy Research. 1991;16: 677– 84.

APPENDICES

$$f_{o(p)}(\eta) = -\left(\frac{n_3}{n_3\left(n_3^2 - n_2 n_3\right)} - \frac{1}{\left(n_3^2 - n_2 n_3\right)}\right)\left(\frac{GrAe^{\lambda_1\eta}}{\lambda_1} + \frac{GrBe^{\lambda_2\eta}}{\lambda_2} + \frac{GrCe^{m_1\eta}}{m_1} + \frac{GrDe^{m_2\eta}}{m_2}\right)$$

$$+\frac{n_3}{n_3\left(n_3^2 - n_2 n_3\right)}\left(\frac{GrAe^{\lambda_1\eta}}{(\lambda_1 - n_2)} + \frac{GrBe^{\lambda_2\eta}}{(\lambda_2 - n_2)} + \frac{GrCe^{m_1\eta}}{(m_1 - n_2)} + \frac{GrDe^{m_2\eta}}{(m_2 - n_2)}\right)$$

$$-\frac{1}{n_3\left(n_3^2 - n_2 n_3\right)}\left(\frac{GrAe^{\lambda_1\eta}}{(\lambda_1 - n_3)} + \frac{GrBe^{\lambda_2\eta}}{(\lambda_2 - n_3)} + \frac{GrCe^{m_1\eta}}{(m_1 - n_3)} + \frac{GrDe^{m_2\eta}}{(m_2 - n_3)}\right)$$

$$\lambda_1 = -\frac{1}{2} + \frac{\sqrt{1-4N^2}}{2},\ \lambda_2 = -\frac{1}{2} - \frac{\sqrt{1-4N^2}}{2}$$

$$\lambda_1 = -\frac{1}{2} + \mu_1, \lambda_2 = -\frac{1}{2} - \mu_1, \mu_1 = \frac{\sqrt{1-4N^2}}{2}$$

$$m_1 = -\frac{1}{2} + \mu_2, m_2 = -\frac{1}{2} - \mu_2, \mu_2 = \frac{\sqrt{1-4\delta_1^2}}{2}$$

$$n_2 = -\frac{1}{2} + \mu_3, n_3 = -\frac{1}{2} - \mu_3, \mu_3 = \frac{\sqrt{1-4M^2}}{2}$$

$$A = \frac{\Theta_w e^{1/2} - e^{\mu_1}}{\sinh\mu_1}, B = \frac{e^{\mu_1} - \Theta_w e^{1/2}}{\sinh\ \mu_1},\ C = \frac{\Phi_w e^{1/2} - e^{\mu_2}}{\sinh\mu_2}, D = \frac{e^{\mu_2} - \Phi_w e^{1/2}}{\sinh\mu_2}$$

$$\Theta_{1(p)}(\eta) = \frac{\Pr}{(\lambda_2 - \lambda_1)}[\ \lambda_1 FAe^{(\lambda_1+n_2)\eta} + \lambda_1 GAe^{(\lambda_1+n_3)\eta}$$

$$-\left(\frac{n_3}{n_2\left(n_3^2 - n_2 n_3\right)} - \frac{1}{\left(n_3^2 - n_2 n_3\right)}\ \right)\left(\begin{array}{l} GrA^2 e^{2\lambda_1\eta} + \frac{\lambda_1 GrABe^{(\lambda_1+\lambda_2)\eta}}{\lambda_2} + \frac{\lambda_1 GcACe^{(\lambda_1+m_1)\eta}}{m_1} \\ + \frac{\lambda_1 GcADe^{(\lambda_1+m_2)\eta}}{m_2} \end{array}\right)$$

$$+\frac{n_3}{n_2\left(n_3^2 - n_2 n_3\right)}\left(\frac{\lambda_1 GrA^2 e^{2\lambda_1\eta}}{(\lambda_1 - n_2)} + \frac{\lambda_1 GrABe^{(\lambda_1+\lambda_2)\eta}}{(\lambda_2 - n_2)} + \frac{\lambda_1 GcACe^{(\lambda_1+m_1)\eta}}{(m_1 - n_2)} + \frac{\lambda_1 GcADe^{(\lambda_1+m_2)\eta}}{(m_2 - n_2)}\right)$$

$$-\frac{1}{\left(n_3^2-n_2n_3\right)}\left(\frac{\lambda_1 GrA^2e^{2\lambda_1\eta}}{\left(\lambda_1-n_3\right)}+\frac{\lambda_1 GrABe^{(\lambda_1+\lambda_2)\eta}}{\left(\lambda_2-n_3\right)}+\frac{\lambda_1 GcACe^{(\lambda_1+m_1)\eta}}{\left(m_1-n_3\right)}+\frac{\lambda_1 GcADe^{(\lambda_1+m_2)\eta}}{\left(m_2-n_3\right)}\right)\ ]+\ldots$$

$$\Phi_{1(p)}(\eta)=\frac{Sc}{(m_2-m_1)}[\ \ m_1FCe^{(m_1+n_2)\eta}+m_1GCe^{(m_1+n_3)\eta}$$

$$-\left(\frac{n_3}{n_2\left(n_3^2-n_2n_3\right)}-\frac{1}{\left(n_3^2-n_2n_3\right)}\ \right)\left(\frac{m_1GrACe^{(\lambda_1+m_1)\eta}}{\lambda_1}+\frac{m_1GrBCe^{(\lambda_2+m_1)\eta}}{\lambda_2}+GcC^2e^{2m_1\eta}+\frac{m_1GcCDe^{(m_1+m_2)\eta}}{m_2}\right)$$

$$+\frac{n_3}{n_2\left(n_3^2-n_2n_3\right)}\left(\frac{m_1GrACe^{(\lambda_1+m_1)\eta}}{\left(\lambda_1-n_2\right)}+\frac{m_1GrBCe^{(\lambda_2+m_1)\eta}}{\left(\lambda_2-n_2\right)}+\frac{m_1GcC^2e^{2m_1\eta}}{\left(m_1-n_2\right)}+\frac{m_1GcCDe^{(m_1+m_2)\eta}}{\left(m_2-n_2\right)}\right)$$

$$-\frac{1}{\left(n_3^2-n_2n_3\right)}\left(\frac{m_1GrACe^{(\lambda_1+m_1)\eta}}{\left(\lambda_1-n_3\right)}+\frac{m_1GrBCe^{(\lambda_2+m_1)\eta}}{\left(\lambda_2-n_3\right)}+\frac{m_1GcC^2e^{2m_1\eta}}{\left(m_1-n_3\right)}+\frac{m_1GcCDe^{(m_1+m_2)\eta}}{\left(m_2-n_3\right)}\right)\ ]+\ldots$$

$$-Gr\ \left\{\frac{\mathrm{J}_1e^{n_1\eta}}{n_2}+\frac{J_2e^{n_2\eta}}{n_2}\ +\frac{\mathrm{Pr}}{\left(\lambda_2-\lambda_1\right)}\left[\frac{\lambda_1FAe^{(\lambda_1+n_2)\eta}}{\left(\lambda_1+n_2\right)}+\frac{\lambda_1GAe^{(\lambda_1+n_3)\eta}}{\left(\lambda_1+n_3\right)}\right.\right.$$

$$-\left(\frac{n_3}{\left(n_3^2-n_2n_3\right)}-\frac{1}{\left(n_3^2-n_2n_3\right)}\right)\left(\frac{GrA^2e^{2\lambda_1\eta}}{2}+\frac{GrBAe^{(\lambda_1+\lambda_2)\eta}}{\left(\lambda_1+\lambda_2\right)}+\frac{\lambda_1GcCAe^{(\lambda_1+m_1)\eta}}{\left(\lambda_1+m_1\right)m_1}+\frac{\lambda_1GcDAe^{(\lambda_1+m_2)\eta}}{\left(\lambda_1+m_2\right)m_2}\right)$$

$$+\frac{n_3}{n_2\left(n_3^2-n_2n_3\right)}\left(\frac{GrA^2e^{2\lambda_1\eta}}{2\left(\lambda_1-n_2\right)}+\frac{\lambda_1GrBAe^{(\lambda_1+\lambda_2)\eta}}{\left(\lambda_2-n_2\right)\left(\lambda_1+\lambda_2\right)}+\frac{\lambda_1GcCAe^{(\lambda_1+m_1)\eta}}{\left(m_1-n_2\right)\left(\lambda_1+m_1\right)}+\frac{\lambda_1GcDAe^{(\lambda_1+m_2)\eta}}{\left(m_2-n_2\right)\left(\lambda_1+m_2\right)}\right)$$

$$-\frac{1}{\left(n_3^2-n_2n_3\right)}\left(\frac{GrA^2e^{2\lambda_1\eta}}{2\left(\lambda_1-n_3\right)}+\frac{\lambda_1GrBAe^{(\lambda_1+\lambda_2)\eta}}{\left(\lambda_2-n_3\right)\left(\lambda_1+\lambda_2\right)}+\frac{\lambda_1GcCAe^{(\lambda_1+m_1)\eta}}{\left(m_1-n_3\right)\left(\lambda_1+m_1\right)}+\frac{\lambda_1GcDAe^{(\lambda_1+m_2)\eta}}{\left(m_2-n_3\right)\left(\lambda_1+m_2\right)}\right)\ ]$$

$$+\ldots\}$$

$$f_{1(p)}(\eta)=\left(\frac{n_3}{n_2\left(n_3^2-n_2n_3\right)}-\frac{1}{\left(n_3^2-n_2n_2\right)}\right)\ \left\{\ \left[Fe^{n_2\eta}+Ge^{n_3\eta}\right.\right.$$

$$-\left(\frac{n_3}{n_2\left(n_3^2-n_2n_3\right)}-\frac{1}{\left(n_3^2-n_2n_3\right)}\ \right)\left(\frac{GrAe^{\lambda_1\eta}}{\lambda_1}+\frac{GrBe^{\lambda_2\eta}}{\lambda_2}+\frac{GcCe^{m_1\eta}}{m_1}+\frac{GcDe^{m_2\eta}}{m_2}\right)$$

$$+\frac{n_3}{n_2\left(n_3^2-n_2n_3\right)}\left(\frac{GrAe^{\lambda_1\eta}}{\left(\lambda_1-n_2\right)}+\frac{GrBe^{\lambda_2\eta}}{\left(\lambda_2-n_2\right)}+\frac{GcCe^{m_1\eta}}{\left(m_1-n_2\right)}+\frac{GcDe^{m_2\eta}}{\left(m_2-n_2\right)}\right)$$

$$-\frac{1}{\left(n_3^2-n_2n_3\right)}\left(\frac{GrAe^{\lambda_1\eta}}{\left(\lambda_1-n_3\right)}+\frac{GrBe^{\lambda_2\eta}}{\left(\lambda_2-n_3\right)}+\frac{GcCe^{m_1\eta}}{\left(m_1-n_3\right)}+\frac{GcDe^{m_2\eta}}{\left(m_2-n_3\right)}\right)\ ]+\ldots$$

$$-\frac{1}{\left(n_3^2-n_2n_3\right)}\left(\frac{GrAe^{\lambda_1\eta}}{\left(\lambda_1-n_3\right)}+\frac{GrBe^{\lambda_2\eta}}{\left(\lambda_2-n_3\right)}+\frac{GcCe^{m_1\eta}}{\left(m_1-n_3\right)}+\frac{GcDe^{m_2\eta}}{\left(m_2-n_3\right)}\right)\ ]$$

$$-\left(\frac{n_3}{\left(n_3^2-n_2n_3\right)}-\frac{1}{\left(n_3^2-n_2n_3\right)}\right)\left(\frac{GrA^2e^{2\lambda_1\eta}}{2}+\frac{GrBAe^{(\lambda_1+\lambda_2)\eta}}{\left(\lambda_1+\lambda_2\right)}+\frac{\lambda_1GcCAe^{(\lambda_1+m_1)\eta}}{\left(\lambda_1+m_1\right)m_1}+\frac{\lambda_1GcDAe^{(\lambda_1+m_2)\eta}}{\left(\lambda_1+m_2\right)m_2}\right)$$

$$+\frac{n_3}{n_2\left(n_3^2-n_2n_3\right)}\left(\frac{GrA^2e^{2\lambda_1\eta}}{2\left(\lambda_1-n_2\right)}+\frac{\lambda_1GrBAe^{(\lambda_1+\lambda_2)\eta}}{\left(\lambda_2-n_2\right)\left(\lambda_1+\lambda_2\right)}+\frac{\lambda_1GcCAe^{(\lambda_1+m_1)\eta}}{\left(m_1-n_2\right)\left(\lambda_1+m_1\right)}+\frac{\lambda_1GcDAe^{(\lambda_1+m_2)\eta}}{\left(m_2-n_2\right)\left(\lambda_1+m_2\right)}\right)$$

$$-\frac{1}{\left(n_3^2-n_2n_3\right)}\left(\frac{GrA^2e^{2\lambda_1\eta}}{2\left(\lambda_1-n_3\right)}+\frac{\lambda_1GrBAe^{(\lambda_1+\lambda_2)\eta}}{\left(\lambda_2-n_3\right)\left(\lambda_1+\lambda_2\right)}+\frac{\lambda_1GcCAe^{(\lambda_1+m_1)\eta}}{\left(m_1-n_3\right)\left(\lambda_1+m_1\right)}+\frac{\lambda_1GcDAe^{(\lambda_1+m_2)\eta}}{\left(m_2-n_3\right)\left(\lambda_1+m_2\right)}\right)\ ]$$

$$+\ldots\quad -Gc\ \left\{\frac{\mathrm{R}_1e^{m_1\eta}}{m_1}+\frac{\mathrm{R}_2e^{m_2\eta}}{m_2}\ +\frac{Sc}{\left(m_2-m_1\right)}\left[\frac{m_1FCe^{(m_1+n_2)\eta}}{\left(m_1+n_2\right)}+\frac{m_1GCe^{(m_1+n_3)\eta}}{\left(m_1+n_3\right)}\right.\right.$$

$$\left(\frac{n_3}{n_2\left(n_3^2-n_2n_3\right)}-\frac{1}{\left(n_3^2-n_2n_3\right)}\right)\left(\frac{m_1GrACe^{\left(m_1+\lambda_1\right)\eta}}{\lambda_1\left(m_1+\lambda_1\right)}+\frac{m_1GrBCe^{\left(m_1+\lambda_1\right)\eta}}{\lambda_2\left(m_1+\lambda_1\right)}+\frac{GcC^2e^{2m_1\eta}}{2m_1}+\frac{m_1GcDCe^{\left(m_1+m_2\right)\eta}}{m_2\left(m_1+m_2\right)}\right)$$

$$-\frac{n_3}{n_2\left(n_3^2-n_2n_3\right)}\left(\frac{m_1GrACe^{\left(m_1+\lambda_1\right)\eta}}{\left(\lambda_1-n_2\right)\left(m_1+\lambda_1\right)}+\frac{m_1GrBCe^{\left(m_1+\lambda_2\right)\eta}}{\left(\lambda_2-n_2\right)\left(m_1+\lambda_2\right)}+\frac{GcC^2e^{2m_1\eta}}{\left(m_1-n_2\right)2}+\frac{m_1GcDCe^{\left(m_1+m_2\right)\eta}}{\left(m_2-n_2\right)\left(m_1+m_2\right)}\right)$$

$$-\frac{1}{\left(n_3^2-n_2n_3\right)}\left(\frac{m_1GrACe^{(m_1+\lambda_1)\eta}}{\left(\lambda_1-n_3\right)\left(m_1+\lambda_1\right)}+\frac{m_1GrBCe^{(m_1+\lambda_2)\eta}}{\left(\lambda_2-n_3\right)\left(m_1+\lambda_2\right)}+\frac{GcC^2e^{2m_1\eta}}{\left(m_1-n_3\right)2}+\frac{m_1GcDCe^{(m_1+m_2)\eta}}{\left(m_2-n_3\right)\left(m_1+m_2\right)}\right)\ ]$$

$+\ldots]\}$

$$E=0$$

$$F = \frac{\left(\quad f_{o(p)}(0)e^{-(\mu_3+1/2)} - f_{o(p)}(1)\right)e^{1/2}}{2\sinh\mu_3}, \qquad G = \frac{-\left(\quad f_{o(p)}(0)e^{-(\mu_3+1/2)} - f_{o(p)}(1)\right)e^{1/2}}{2\sinh\mu_3} - f_{o(p)}(0)$$

$$J_1 = \frac{e^{\alpha x/2}\left(\gamma_1\Theta_w - \Theta_{1(p)}(\alpha x) + \Theta_{1(p)}(0)e^{-(\mu_1+1/2)\alpha x}\right)}{2\sinh(\mu_1\alpha x)}, \qquad J_2 = \frac{-e^{\alpha x/2}\left(\gamma_1\Theta_w - \Theta_{1(p)}(\alpha x) + \Theta_{1(p)}(0)e^{-(\mu_1+1/2)\alpha x}\right)}{2\sinh(\mu_1\alpha x)} - \Theta_{1(p)}(0)$$

$$R_1 = \frac{e^{\alpha x/2}\left(\gamma_2\Phi_w - \Phi_{1(p)}(\alpha x) + \Phi_{1(p)}(0)e^{-(\mu_2+1/2)\alpha x}\right)}{2\sinh(\mu_2\alpha x)}, \qquad R_2 = \frac{-e^{\alpha x/2}\left(\gamma_2\Phi_w - \Phi_{1(p)}(\alpha x) + \Phi_{1(p)}(0)e^{-(\mu_2+1/2)\alpha x}\right)}{2\sinh(\mu_2\alpha x)} - \Phi_{1(p)}(0)$$

Peer-review history:
The peer review history for this paper can be accessed here:
http://sciencedomain.org/review-history/17387